

CHANG-ES VII:
MAGNETIC OUTFLOWS FROM THE VIRGO CLUSTER GALAXY NGC 4388

A. DAMAS-SEGOVIA¹, R. BECK¹, B. VOLLMER², T. WIEGERT³, M. KRAUSE¹, J. IRWIN³, M. WEŻGOWIEC⁴, J. LI⁵, R.-J. DETTMAR⁶, J. ENGLISH⁷, Q. D. WANG⁸

¹MPI für Radioastronomie, Auf dem Hügel 69, 53121 Bonn, Germany

²Observatoire astronomique de Strasbourg, Université de Strasbourg, CNRS, UMR 7550, 11 rue de l'Université, 67000 Strasbourg, France

³Dept. of Physics, Engineering physics & Astronomy, Queen's University, Kingston, ON, Canada, K7L 3N6

⁴Observatorium Astronomiczne Uniwersytetu Jagiellońskiego, ul. Orła 171, 30-244 Kraków, Poland

⁵Dept. of Astronomy, University of Michigan, 311 West Hall, 1085 S. University Ave., Ann Arbor, MI 48109, USA

⁶Astronomisches Institut, Ruhr-Universität Bochum, 44780 Bochum, Germany

⁷Department of Physics and Astronomy, University of Manitoba, Winnipeg, Manitoba, R3T 2N2, Canada

⁸Dept. of Astronomy, University of Massachusetts, 710 North Pleasant St., Amherst, MA, 01003, USA

ABSTRACT

We investigate the effects of ram pressure on the ordered magnetic field of a galaxy hosting a radio halo and strong nuclear outflows. New radio images in total and polarized intensity of the edge-on Virgo galaxy NGC 4388 were obtained within the CHANG-ES EVLA project. The unprecedented noise level reached allows us to detect striking new features of the ordered magnetic field. The nuclear outflow extends far into the halo to about 5 kpc from the center and is spatially correlated with the H α and X-ray emission. For the first time, the southern outflow is detected. Above and below both spiral arms we find extended blobs of polarized emission with an ordered field oriented perpendicular to the disk. The synchrotron lifetime of the cosmic ray electrons (CREs) in these regions yields a mean outflow velocity of $(270 \pm 70) \text{ km s}^{-1}$, in agreement with a galactic wind scenario. The observed symmetry of the polarized halo features in NGC 4388 excludes a compression of the halo gas by the ram pressure of the intra-cluster medium (ICM). The assumption of equilibrium between the halo pressure and the ICM ram pressure yields an estimate of the ICM density that is consistent with both the ICM density derived from X-ray observations and the recent *Planck* Sunyaev-Zel'dovich measurements. The detection of a faint radio halo around cluster galaxies could thus be used for an estimate of ICM ram pressure.

Subject headings: galaxies: individual: NGC 4388 – galaxies: clusters: individual: Virgo Cluster – galaxies: halos – galaxies: intergalactic medium – galaxies: jets – galaxies: magnetic fields

1. INTRODUCTION

NGC 4388 is an almost edge-on SA(s)b galaxy (inclination 79°) in the Virgo cluster (at about 17 Mpc distance), located about 1.3° (≈ 400 kpc) west from the center of the cluster (Chung et al. 2009). The interstellar medium (ISM) of NGC 4388 has undergone a stripping event by ram pressure, evident from the rapid decline of star formation (190 ± 30) Myr ago (Pappalardo et al. 2010). Like many other galaxies in cluster environments, NGC 4388 is a H I-deficient galaxy that lost about 85% of its H I mass (Cayatte et al. 1990). The H I disk is strongly truncated within the optical disk. An H I plume extends up to 100 kpc out from the galaxy plane (Oosterloo & van Gorkom 2005). The gas stripping is possibly the result of the interaction between the galaxy and the ICM. Vollmer & Huchtmeier (2003) estimated that the galaxy passed close to the cluster center about 120 Myr ago. A more recent model yields a timescale of about 200 Myr (Vollmer, priv. comm.).

Early VLA studies of this galaxy revealed a bright double source in the nucleus and an outflow lobe that opens up like an hourglass and extends to about 1.5 kpc from the center (Hummel et al. 1983; Hummel & Saikia 1991; Kukula et al. 1995; Falcke et al. 1998). Observations

with very-long-baseline interferometry (VLBI) revealed a radio jet with $\cong 0.5$ pc extent (Giroletti & Panessa 2009). A circumnuclear disk of $\cong 0.1$ pc radius, oriented edge-on and almost parallel to the galaxy plane, was detected by its water maser emission (Kuo et al. 2011). This indicates that the jet and the outflow emerge almost perpendicular to the galaxy plane.

Previous VLA and Effelsberg radio continuum observations showed an extended halo and extended features out of the disk (Vollmer et al. 2010; Weżgowiec et al. 2012). These features may be related to the outflow event seen in H α and O III observations (Yoshida et al. 2002, 2004).

These deep optical spectroscopic observations are crucial to understanding the complexity and the dynamics of the outflow of ionized gas from this galaxy. Yoshida et al. (2002) concluded that the extended emission-line region is gas stripped by the action of ram pressure and photoionized by the radiation from the AGN.

High resolution X-ray observations with *Chandra X-ray Observatory* show emission from the outflow as well as from the radio jet (Iwasawa et al. 2003). On the other hand, lower resolution X-ray observations with XMM-Newton reveal the hot halo surrounding this galaxy. This halo might be shaped by the Mach cone created by the supersonic speed of the galaxy in that medium (Weżgowiec et al. 2011). The clear correlation between

TABLE 1
NGC 4388 PROPERTIES

R.A. (J2000)	12 ^h 25 ^m 46.75 ^s
Dec. (J2000)	12 ^d 39 ^m 43.5 ^s
Type	SA(s)b
Inclination ^a	79°
Position angle	92°
d_{25} ^b	5.6'
Distance	17 Mpc

^aInclination, $i = 3 \text{ deg} + \cos^{-1}(\sqrt{((b/a)^2 - 0.2^2)/(1 - 0.2^2)})$, where b/a is the minor to major axis ratio.

^bObserved blue diameter at the 25th mag arcsec⁻² isophote.

features in optical, radio and X-ray frequencies suggests a common origin.

The distribution of polarized radio emission in a cluster galaxy tends to be asymmetric as a consequence of interaction with the ICM (Vollmer et al. 2007, 2013). This interaction enhances the polarized flux on the side which is facing the ram pressure due to the motion of the galactic disk in the denser environment. The H I plume detected by Oosterloo & van Gorkom (2005) represents clear evidence of interaction between the galaxy and the ICM of Virgo toward the southern part of its disk.

Little is known so far about the role of magnetic fields in the outflows of NGC 4388. Polarized radio emission is a signature of ordered magnetic fields. Previous low-resolution Effelsberg observations by Weżgowiec et al. (2012) showed a large-scale magnetic field that is inclined with respect to the disk plane. Higher-resolution VLA observations by Vollmer et al. (2010) show a complex magnetic field structure which is different in the outflow, the disk and the halo.

Vollmer (2009) performed simulations with a sticky particle code (Vollmer et al. 2001) to quantify the outflow event that takes place in NGC 4388. They were able to reproduce with high fidelity the direction, speed and density of the stripped gas. An important part of that study was to observe the evolution of the ram pressure of the ICM as a function of time. In that model the predicted ram pressure at the current stage of the galaxy's orbit is in a decreasing phase. They estimated a ram pressure of $1 \times 10^{-11} \text{ dyn cm}^{-2}$ at the present time. Within this scenario, it is expected that the action of ram pressure would transform the morphology of the gaseous galactic halo. The side of the galaxy facing ram pressure would be compressed leading to a sharp smooth edge of the radio continuum emission, with no extensions toward the outskirts of the halo.

We intend to investigate the impact of ram pressure on the magnetic field of NGC 4388 with help of the new radio polarization observations. In particular, wide-band polarimetric studies are of crucial importance for this purpose, since they reach lower limits of rms and therefore allow us to detect faint structures out in the halo of a galaxy where a weaker magnetic field is expected. In the current study we make use of improved instruments and new techniques. Higher resolution and sensitivity reveal many details of the magnetic field structure of NGC 4388 that were never observed before. New features of the galactic magnetic field in NGC 4388 extending up to 5 kpc out in the halo on both sides of the galactic disk are revealed. They are in conflict with models that include a continuous smooth ICM density profile

TABLE 2
DETAILS OF VLA OBSERVATIONS

Dates of observations	19 Dec 2011 and 08 Apr 2012
Configurations	C, D
Central frequency	6.0 GHz
Bandwidth	2.0 GHz
Spectral channels per window	64
Channel width	2 MHz
Spectral windows	16
Primary calibrator	3C286
Secondary calibrator	J1254+1141
Polarization leakage calibrator	J1407+2827

which predict an asymmetric gas distribution within the galactic halo due to ISM compression.

In Sect. 2 we present the observations and the data reduction. Images of radio total power and polarized emission as well as an analysis of the magnetic field of NGC 4388 can be found in Sect. 3. A discussion on the different features seen in these new observations follows in Sect. 4. We suggest in Sect. 4.6 that ICM clumpiness as a possible explanation for the discrepancy between the ram pressure derived from observations and predicted by dynamical models. Sect. 5 contains a summary of the main points of the present study.

2. OBSERVATIONS AND DATA REDUCTION

As a part of the CHANG-ES project (Continuum Halos in Nearby Galaxies - an EVLA Survey; Irwin et al. 2012), the data set presented here was observed in C band (5–7 GHz) with the the Karl G. Jansky Very Large Array (VLA) in D configuration (Wiegert et al. 2015) and C configuration (this paper). Details of the observations are given in Table 2. The large bandwidth at this frequency gives a high sensitivity never reached before in imaging of galaxies and allows the application of the RM (rotation measure) Synthesis technique (Brentjens & de Bruyn 2005; Heald 2009, 2015) that increases the signal to noise ratio of the polarized intensity images compared to previous studies.

By combining the datasets of both array configurations we improved the uv coverage and the signal-to-noise ratio substantially.

L-band data (1–2 GHz) were also obtained as part of the CHANG-ES project, but unfortunately the data sets in this frequency band reveal large rms noise values for the NGC 4388 field. This is due to the fact that this galaxy is very close to the Virgo cluster core in the plane of the sky ($\approx 1^\circ$) and therefore cleaning residuals from M87, which is the central source of this cluster, increase the noise. M84, a radio galaxy which lies right at the edge of the primary beam at this frequency range, also increases the noise of these observations. In addition, no polarization was found in the L band datasets probably due to a stronger depolarization effect by Faraday dispersion at these frequencies and higher noise.

The data reduction was done using the Common Astronomy Software Applications package (CASA¹). Radio frequency interference (RFI) flagging and calibration was performed for each individual channel. Imaging in Stokes I was done averaging the entire band of the dataset while imaging in Q and U was done for each of the 16 spectral

¹<http://casa.nrao.edu/>

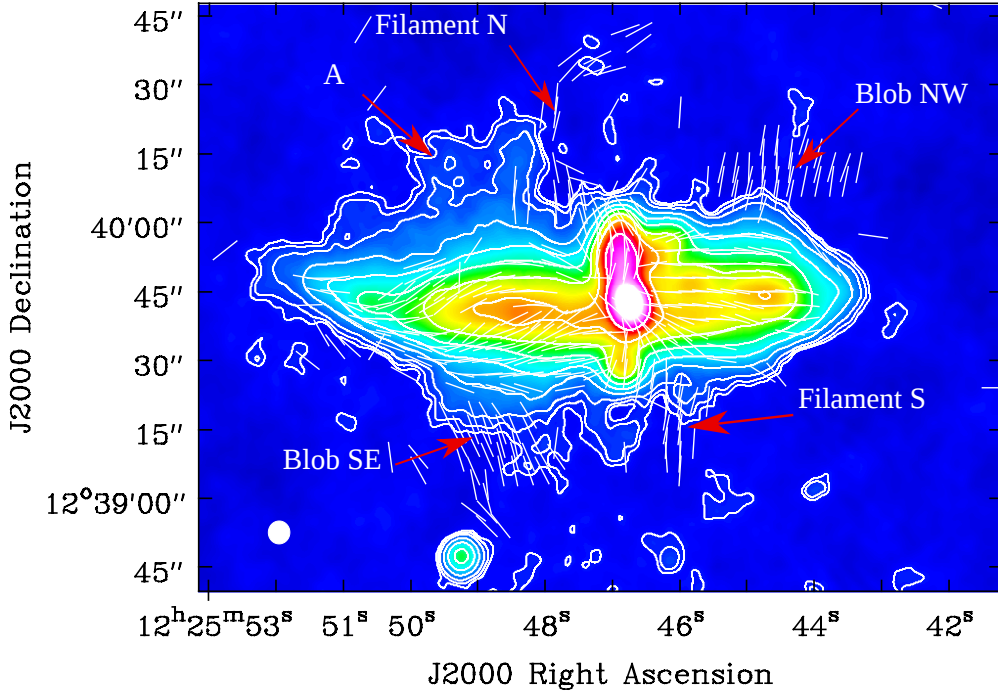


FIG. 1.— Total intensity at 6 GHz in contours plus magnetic vectors with the same vector length, corrected for Faraday rotation, with a resolution of $4.99'' \times 4.69''$ and an rms noise of $3.5 \mu\text{Jy}/\text{beam}$. The contour levels are $(3, 4, 6, 12, 24, 48, 96, 200, 500) \times 3.5 \mu\text{Jy}/\text{beam}$. A combination of the data from the C and D configurations of the VLA was used to make the total intensity map whereas only C configuration data was necessary to create the map of magnetic vectors. Both maps have been cleaned with a robust 2 weighting. The galaxy moves in the SW direction.

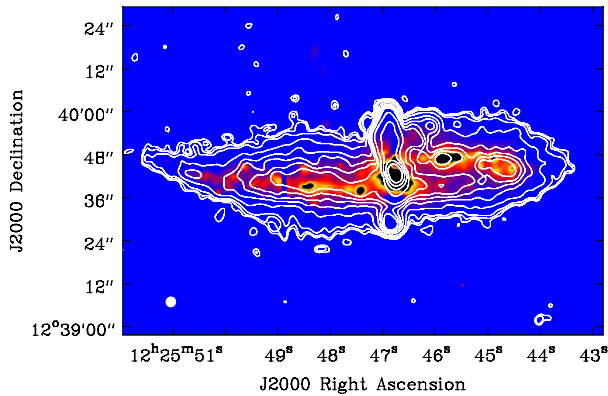


FIG. 2.— Total intensity contours plotted over $\text{H}\alpha$ map from Yoshida et al. (2002). Contours are $(3, 4, 6, 12, 24, 36, 48, 64, 128, 256, 512, 1024) \times 3.3 \mu\text{Jy}/\text{beam}$. This map was made with data of C configuration with robust 0 weighting. The resolution of the radio total intensity is $2.76'' \times 2.67''$ and the rms noise is $3.3 \mu\text{Jy}/\text{beam}$.

windows to be combined into a cube. Natural weighting (robust = 2) was used during the cleaning process to ensure a higher sensitivity to extended emission. Due to the good quality data only two runs of selfcalibration were made, one in phase and a second one in amplitude and phase.

For the first time for this galaxy, the polarization products of this dataset were obtained by applying the RM Synthesis method (Brentjens & de Bruyn 2005) to the 15 images of the usable spectral windows of 128 MHz each in Stokes Q and U. One window was removed due to low signal-to-noise ratios. Each individual spectral window image was smoothed to the resolution of the spectral window with the lowest resolution and corrected for primary beam attenuation. RM Synthesis allows us to recover most of the polarized emission that would be lost due to bandwidth depolarization while averaging Q and U intensities over the whole bandwidth. The final polarized intensity map was obtained from the Q and U values at the maximum intensity peaks in the Faraday spectrum at each pixel in the sky plane. The bias generated in polarized intensity was then subtracted. Thanks to this technique we reach a noise of $2.3 \mu\text{Jy}/\text{beam}$ at a resolution of $5.33'' \times 5.33''$ with an observation of 180 minutes on the target source (before flagging). To our knowledge, this is the lowest rms for a polarization map yet accomplished for an external galaxy.

The wavelength coverage of our observations in the given wavelength range ($\Delta\lambda^2$) gives a resolution in Faraday space of $\delta\phi \cong 2000 \text{ rad m}^{-2}$, which is sufficient to distinguish components in the Faraday spectrum that are separated by more than $\delta\phi/(2S/N)$, where S/N is the signal-to-noise ratio of the polarized intensity. As Faraday depth of a few 100 rad m^{-2} are not expected from emitting regions along the line of sight through galaxies,

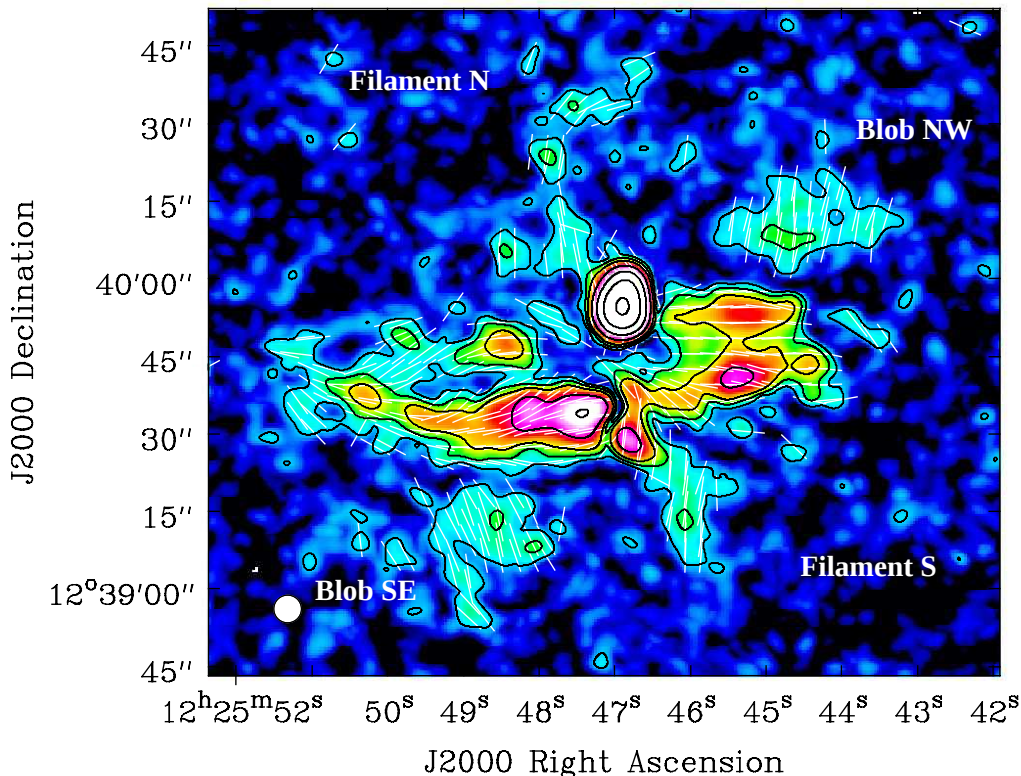


FIG. 3.— Linearly polarized intensity at 6 GHz in contours plus magnetic vectors with the same vector length, corrected for Faraday rotation, with a resolution of $5.33'' \times 5.33''$ and an rms noise of $2.3 \mu\text{Jy}/\text{beam}$. The contour levels are $(3, 5, 8, 16, 32, 64, 128) \times 2.3 \mu\text{Jy}/\text{beam}$. Both maps have been cleaned with a robust 2 weighting.

we presume that we detect only one Faraday component at all locations.

3. RESULTS

3.1. Images in total and polarized intensity

The total intensity image obtained by combining D and C array observations from CHANG-ES show new details in the morphology of this galaxy (see Fig. 1). The prominent jet-like structure just north of the nucleus is clearly detected, as in previous works (Hummel & Saikia 1991; Kukula et al. 1995; Falcke et al. 1998), but now the disk is seen with higher resolution and sensitivity. The high surface brightness disk ($\approx 700 \mu\text{Jy}/\text{beam}$) of these new observations is quite symmetric including two spiral arms (the northwestern arm being closer to us) observed in $\text{H}\alpha$ (Yoshida et al. (2002, 2004); Fig.2). At intermediate surface brightness ($\approx 40 \mu\text{Jy}/\text{beam}$) we observe a pointed tail to the east (on the far east end of the galaxy) which bends toward the north. The southern part of that tail shows a sharp edge. A low surface brightness ($\approx 10 \mu\text{Jy}/\text{beam}$) diffuse halo is also detected. The halo is more extended and patchy in the eastern side of the galaxy. In the northeastern region (see region marked as A in Fig. 1) we find a similar structure between the total intensity radio emission and the $\text{H}\alpha$ outflow.

Figure 3 shows the polarized emission of NGC 4388. The total power jet-like structure is also prominent in polarization. We detect strong polarized emission within the total power disk. The polarized intensity is strongest between the spiral arms as commonly observed in spi-

ral galaxies (Beck & Wielebinski 2013). The rms noise in the polarized maps is lower than in the total intensity maps, therefore we are able to see many details in polarization that are not revealed in total power. Extended new features in polarized emission are discovered far away from the disk. Two almost vertical filaments have projected extensions of $50''$ ($\cong 4.1 \text{ kpc}$) to the north and $20''$ ($\cong 1.7 \text{ kpc}$) to the south. Other intriguing features of these new observations are the two extended extra-planar regions of polarized emission at large distances ($\approx 3.7 \text{ kpc}$) northwest and southeast from the galaxy center. In the following we will call these features the northwestern and southeastern blobs. They reveal an ordered magnetic field and CREs about 5 kpc projected distance from the plane of the galaxy.

3.2. The magnetic field in NGC 4388

Figure 1 shows magnetic vectors in the disk parallel to the major axis as expected for edge-on galaxies (Krause 2011). In the southeastern part of the disk the polarization vectors are no longer parallel to the disk and run along the sharp edge of the total power emission. Vertical magnetic vectors can be seen in the central region along the jet-like structure. All magnetic field vectors outside the high and intermediate surface brightness of total power emission are almost vertical with respect to the galactic disk.

Using the revised equipartition formula by Beck & Krause (2005), we calculated the ordered and total magnetic field strengths from the polarized

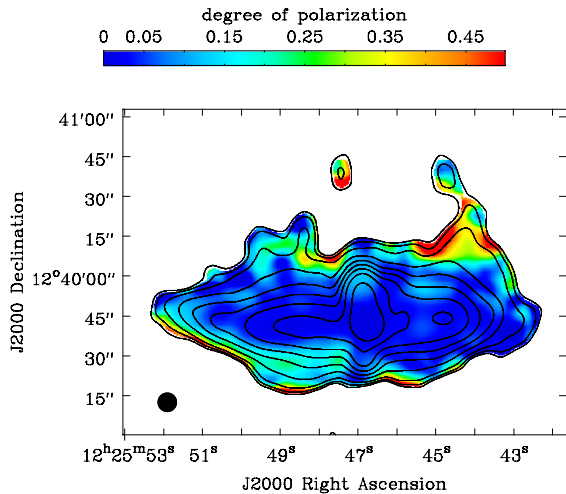


FIG. 4.— Contours of total intensity emission plotted with degree of polarization in colour scale. Contours of total intensity emission are $(3, 4, 6, 12, 24, 48, 96, 200, 500) \times 6 \mu\text{Jy}/\text{beam}$. The resolution is $7'' \times 7''$ and the rms noise is $6 \mu\text{Jy}/\text{beam}$.

and total intensities, respectively. We assumed different path lengths and synchrotron spectral indices for the various parts of the galaxy (see Table 3). The path-lengths through the emitting medium along the line of sight are taken to be the same as the widths of the features in the sky plane. The ratio between the number densities of cosmic ray protons and electrons in the relevant energy range of a few GeV is assumed to be $K = 100$. This value may be larger in the halo due to energy losses of CREs (see Sect. 4.4).

We discuss the possibility of a larger proton-to-electron ratio K than the value of 100 assumed to derive the values in Table 3. The total equipartition magnetic field B_{eq} depends on K as follows (Beck & Krause 2005):

$$B_{\text{eq}} \propto K_{\text{eq}}^{1/(3+\alpha)}, \quad (1)$$

where B_{eq} and K_{eq} are the total magnetic field and the proton to electron ratio from equipartition, respectively. In the absence of a cosmic ray source in the halo, we expect a steep spectral index ($\alpha > 1$ assuming $S_\nu \propto \nu^{-\alpha}$). Therefore, magnetic strength depends on K_{eq} in the following way: $B \propto K_{\text{eq}}^{1/4 \dots 1/5}$. Thus, the magnetic field strength is not very sensitive to K_{eq} . An uncertainty in K_{eq} of a factor of 2 leads to an error in B of about 20%.

We also considered different spectral index values for the various parts of the galaxy. Large deviations in this parameter will not significantly change the final values of the computed magnetic field strength. The resulting field strengths in the disk are consistent with typical values for a spiral galaxy (Beck 2001). For the two blobs (NW and SE), B_{tot} was estimated by using a mean degree of polarization for the NW blob of $p \cong 40 \pm 10\%$ derived from Fig. 4 and assuming a similar degree of polarization for the SE blob. The uncertainty in p introduces an error in B_{tot} of about 10%.

The intrinsic degree of polarization p_0 in the NW blob may be larger if Faraday depolarization occurs there, possibly by H α clouds similar to those observed in the north-east by Yoshida et al. (2002). A turbu-

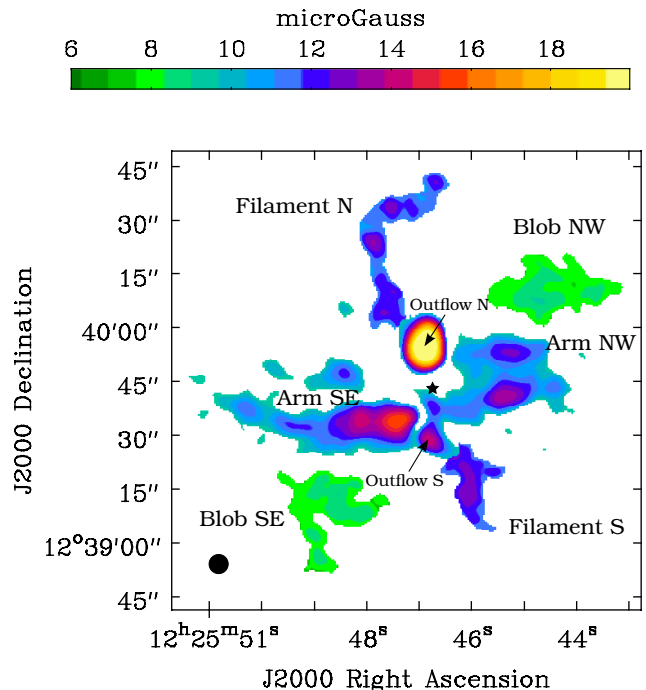


FIG. 5.— Strengths of the ordered field computed from the map of polarized intensities using the revised equipartition formula by Beck & Krause (2005). The nucleus of the galaxy is marked with a star.

lent field strength $B_{\text{turb}} = \sqrt{B_{\text{tot}}^2 - B_{\text{ord}}^2} \cong 8 \mu\text{G}$, a pathlength of about 2300 pc (Table 3), an rms thermal electron density of about 0.35 cm^{-3} in H α clouds of about 200 pc size and 2×10^{-3} volume filling factor (Yoshida et al. 2002) lead to a dispersion in rotation measure of $\sigma_{\text{RM}} \cong 70 \text{ rad m}^{-2}$. The resulting depolarization at 6 GHz by internal Faraday dispersion (e.g. Sokoloff et al. 1998; Arshakian & Beck 2011) is negligible ($p/p_0 \cong 0.97$). Faraday depolarization by hot gas in the halo of NGC 4388 is even less significant because its electron density is only few times 10^{-3} cm^{-3} (Weżgowiec et al. 2011).

The strengths of the ordered field obtained from the polarization map are lower limits, since this emission only represents the component of the magnetic vector in the plane of the sky. If the ordered field is inclined by, say, 30° with respect to the line of sight, its strength would increase by 11%.

Figure 5 shows the strengths of the ordered magnetic field obtained from the map of polarized intensities of NGC 4388. The strength of the ordered magnetic field within the disk is comparable to that of other spiral galaxies. The highest ordered field strengths in the extraplanar region are observed in the vertical filaments. It is notable that the magnetic field in the NW and SE blobs is weaker than in the filaments although the polarized intensities are similar. This is due to the different pathlengths chosen for each region (see Sect. 4.2).

4. DISCUSSION

4.1. Nuclear outflow

We clearly detect the northern outflow extending from the center of NGC 4388 in total intensity (Fig. 1), while the southern counterpart is weaker. Due to the inclina-

TABLE 3
EQUIPARTITION FIELD STRENGTHS IN NGC 4388

	L (kpc)	α	$B_{\text{ord}} (\mu\text{G})$	$B_{\text{tot}} (\mu\text{G})$
Nucleus	1.0	0.8	-	67
Outflow N	1.0	0.8	23	45
Outflow S	1.0	0.8	14	30
Arm/disk SE	1, 4 ^a	0.8	16	23
Arm/disk NW	1, 4 ^a	0.8	13	21
Blob NW	2.3	1.0	9	11 ^b
Blob SE	2.3	1.0	9	11 ^b
Filament N	0.5	1.0	13	-
Filament S	0.5	1.0	13	-

^aThe path-length through the spiral arm is used for polarization, the path-length through the inclined disk for total intensity.

^bEstimated from the degree of polarization of Fig. 4.

tion of the galaxy, the emission from the northern outflow travels through the disk on the way to the observer, contrary to the emission of the southern counterpart. It is common in AGN observations to see one side of the jet brighter than the other due to Doppler beaming (Pearson & Zensus 1987; Kellermann et al. 2007). The blue-shifted velocities of the H α outflow in the north indicate that the northern outflow is pointing toward the observer. In those cases, the jet has an inclination toward the observer and it travels at relativistic speed. This high speed would imply a difference in size between northern and southern polarization filaments due to relativistic effects. However, the AGN jet cannot remain relativistic until kilo-parsec scales. A possible explanation for this configuration would imply an internal asymmetry in the ISM density close to the AGN core. This situation is supported by O III observations (Falcke et al. 1998) where there is a region of diffuse emission toward the south of the nucleus, possibly due to an interaction between the AGN outflow and the ISM gas.

In the northeastern part of the halo we can identify total power emission associated with the outflows in H α and O III (Yoshida et al. 2002, 2004) and X-rays (Iwasawa et al. 2003).

The northern outflow shows strongly polarized emission at the top with degrees of polarization of 12% (Fig. 4), while the central part of the same structure, i.e., the nuclear region of the galaxy, reveals no detectable polarization (< 1%). As the outflow is oriented almost perpendicular to the galaxy disk, Faraday depolarization could occur in the northern (nearby) part of the disk that is located between the outflow and the observer. Strong depolarization ($p/p_0 < 0.1$) at 6 GHz by external Faraday dispersion requires a dispersion in rotation measure of $\sigma_{\text{RM}} > 400 \text{ rad m}^{-2}$, e.g. by a diffuse ionized medium with an average thermal electron density of $> 0.03 \text{ cm}^{-3}$, assuming a turbulent field strength in the disk of $B_{\text{turb}} \cong 15 \mu\text{G}$ (Table 3), a pathlength through the disk of about 5000 pc, 100 pc turbulence length and a volume filling factor of 0.5. Such electron densities are typical for the ISM of spiral galaxies (e.g. Beck 2007). Alternatively, depolarization could occur by internal Faraday dispersion in the outflow itself. For a turbulent field strength of $B_{\text{turb}} \cong 50 \mu\text{G}$ and a pathlength of 1000 pc, an average internal thermal electron density of $> 0.05 \text{ cm}^{-3}$ is needed, which is a reasonable value.

Thanks to the new polarized emission maps, we are

able to identify for the first time the counter-outflow toward the south. The main indication is the change of the orientation of the magnetic vectors from parallel to the spiral arms of the disk to being oriented along the nuclear outflow in the southern part that is connected to the center of the galaxy (Fig. 1). This is a clear indication of a different structure in front of the southern arm. The degree of polarization in the southern outflow is 8%, similar to the outer part of the northern outflow. Contrary to the central northern outflow, the southern outflow does show polarization, probably because the southern spiral arm does not obstruct the view of the southern outflow by the observer.

4.2. NGC4388: not an M82-like superwind

The particular configuration of filaments and blobs seen in polarized radio continuum and H α emission of NGC 4388 might suggest that these are different parts of the same event. Both filaments and blobs seem to form an hourglass-shaped structure. This kind of structure is typically seen in starburst galaxies. The prototypical starburst galaxy M 82 shows such an hourglass shape in H α emission. In such a case, strong star formation in the galactic center and subsequent supernova explosions eject gas into the galactic halo within a biconical structure (Strickland et al. 2002). Hot tenuous gas expands as a superbubble into the halo pushing the extraplanar disk to larger galactic radii and compressing it. The compressed gas cools radiatively and becomes visible in many frequency ranges, leading to the observed hourglass shape. Due to gas compression the magnetic field is enhanced and aligned, giving rise to a large scale ordered magnetic field observed as polarized radio continuum emission (e.g. NGC 5775 Soida et al. 2011). Within this picture the compressed shells should also be visible in X-rays (M 82 Ranalli et al. 2008, NGC 253 Dahlem 1997, NGC 5775 Li et al. 2008). Observations of the diffuse X-ray emission of M 82 (Strickland et al. 1997) show that the superbubble in this galaxy is partly filled with hot ($\gtrsim 10^6 \text{ K}$) gas. The radio continuum emission of M 82 (Adebahr et al. 2013) is co-spatial with the H α and the X-ray emission. In NGC 5775 the diffuse X-ray emission (Li et al. 2008) fills the radio continuum superbubble on the southwestern quadrant of the disk (Soida et al. 2011). The observed correlation between X-rays, H α , and radio continuum indicates that the hot X-ray plasma is closely linked to cooler and denser gas detected in H α and to CREs. Such filaments extend into the galactic halo up to $\cong 10 \text{ kpc}$ in the case of NGC 253 (Strickland et al. 2002).

In NGC 4388 the situation is different. The X-ray emission (see right panel of Fig. 6) is not symmetric as expected from superwind models. Compared to the X-ray emission of NGC 253 we do not see enhanced extraplanar X-ray emission south of the galactic disk, in the area where the base of the bubble should be found. North of the galactic disk there is extraplanar X-ray emission. However, it is very asymmetric with almost all X-ray emission coming from the northeastern side of the galactic disk. In addition, the polarized radio continuum emission shows a filamentary structure as expected by a galactic outflow (Soida et al. 2011) only in the northeastern and the southwestern quadrants. Moreover, the observed SE and NW blobs are elongated parallel to the

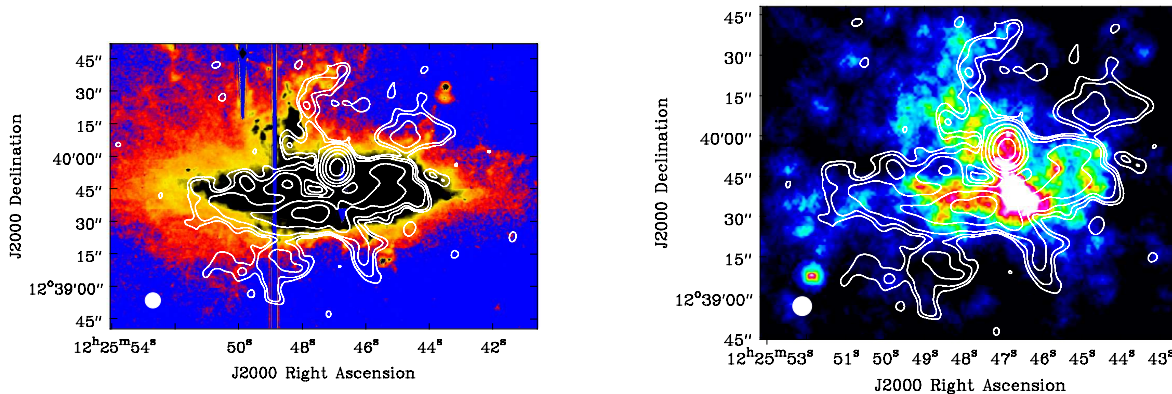


FIG. 6.— Left: Polarized emission obtained with RM Synthesis compared to H α observations from Yoshida et al. (2002). Contours of polarized emission are $(5, 6, 8, 16, 32, 64, 128) \times 2 \mu\text{Jy}/\text{beam}$. The resolution is $7'' \times 7''$ and the rms noise is $2 \mu\text{Jy}/\text{beam}$. Right: Same polarized emission contours over CHANDRA X-ray map from Iwasawa et al. (2003).

disk. Therefore, we conclude that the observed spatial distribution of polarized radio continuum, H α and X-ray emission is not consistent with a symmetric superwind scenario. In Sect. 4.4 we show that NGC 4388 hosts a less prominent galactic wind probably originating from the spiral arms.

4.3. Origin of the polarization filaments

We detect faint polarized emission filamentary in structure extending beyond the end of both sides of the outflow. There are striking similarities in morphology between these features and the H α outflow (left panel of Fig. 6). The polarized radio continuum filaments are offset from the H α plumes toward the minor axis of the galaxy. The projected lengths of these filamentary structures are about $50''$ (4.1 kpc) and $20''$ (1.7 kpc) for the northern and southern parts, respectively. In both cases the deconvolved half power width is about $3.9''$ (0.3 kpc). The symmetry of the two filaments with respect to the galaxy center suggests a collimated outflow perhaps driven by a radio jet. The position angle of the filament is about $20^\circ - 30^\circ$, i.e. it is not perpendicular to the disk plane. The magnetic field vectors show an ordered field along both filaments (see Fig. 3). None of these external features are seen in total intensity due to the lower noise in the polarization maps.

The magnetic field vectors in the southern part connect the nucleus with the southern polarization filament through an apparently wiggling structure. This change of direction could be due to precession event of the AGN jet. In that case, the polarization filaments we see at kiloparsec scales are the continuation of a structure that originates in the nucleus. The fact that there is a drastic drop in polarized intensity between the nuclear outflows and the filaments could be the result of an abrupt change in the direction of the outflow giving rise to this change in polarized intensity. In that case, what we see are different parts of the same event. The origin of the filaments of NGC 4388 will be discussed in more detail in a future

paper.

4.4. Origin of the polarization blobs in the halo

We observe two blobs of polarized emission far out in the galactic halo (about 2 kpc from the disk plane), in the northwestern and southeastern regions above and below the disk, with magnetic field vectors forming an almost vertical field structure (Fig. 1 and 3). The magnetic field vectors within the disk and in the halo are perpendicular to each other, so that there are two areas between the blobs and the disk of low polarization due to geometrical depolarization within the beam. The vertical field in the blobs can be part of a large-scale halo field or field loops stretched by a strong galactic wind (see Sect. 4.6). These polarized blobs remain undetected at other frequencies, e.g., optical, H α , or X-rays. However, some of the channel maps of the H I cubes from Chung et al. (2009) show structures that extend from the outskirts of the western part of the H I disk in the northeastern direction, coincident with the NW blob, indicating a possible relation to the blobs detected in polarization. We interpret this as a galactic outflow from the spiral arms. The fact that the polarized blobs are detected close to both spiral arms in projection ($\approx 15''$) may indicate that they are related to the disk. Furthermore, there is X-ray (see right panel of Fig. 6), polarized and total power emission extending $\approx 10''$ south of the southeastern spiral arm and north of the northwestern spiral arm. If so, possibly the CREs are transported by the galactic wind from the spiral arm. In this case, we estimate the speed of the galactic wind using CREs synchrotron lifetime (e.g. Beck & Wielebinski 2013):

$$t_{\text{syn}} \cong 1.06 \times 10^9 \text{ yr} \left(\frac{B}{\mu\text{G}} \right)^{-\frac{3}{2}} \left(\frac{\nu}{\text{GHz}} \right)^{-\frac{1}{2}} \cong (12 \pm 3) \text{ Myr} \tag{2}$$

where $B \cong 11 \mu\text{G}$ is the total magnetic field (Table 3) with an estimated error of about $2 \mu\text{G}$, and $\nu \cong 6.0 \text{ GHz}$ is the central observation frequency. The distance between the spiral arm and the outer edge of the blobs (at

the level of 5σ) is about $35'' \cong 2.9$ kpc for the NW blob and about $45'' \cong 3.7$ kpc for the SE blob. To reach this height, CREs have to travel with an average velocity of $v \cong (270 \pm 70) \text{ km s}^{-1}$, which is typical for the speed of galactic winds (e.g. Heesen et al. 2009; Arribas et al. 2014). The true speed in the blob depends on the velocity profile of the outflow and could be several times larger, at least by a factor of two for constant acceleration.

The velocity of about 270 km s^{-1} refers to the component of the galactic wind in the sky plane. With a disk inclination of 79° and assuming an outflow velocity vertical to the disk plane, we can estimate the component parallel to the line of sight of that vector and compare it to the observed radial velocities in H α . We estimate the radial velocity of the outflow to be $\approx 60 \text{ km s}^{-1}$, which is close to the value observed in H α (Veilleux et al. 1999). Although there is no stringent reason for the same velocity of the hot (or CREs) and the H α -emitting cool gas flows, it is remarkable that these two components have similar velocities.

The magnetic field computed by the equipartition formula ($11 \mu\text{G}$) could be underestimated. The energy spectrum of CREs propagating into the halo is steepened by energy losses and hence is not proportional to the proton spectrum, i.e. the proton-to-electron ratio K is significantly larger than 100 as assumed in Sect. 3.2 (see discussion in Beck & Krause 2005). In this case we would get a shorter synchrotron lifetime and therefore a larger velocity of the outflow. A better estimate of the outflow speed needs knowledge of the synchrotron spectral index as a function of height above the plane, which cannot be obtained with the present data.

It is surprising that there is no counterpart of both blobs on the opposite sides of the disk in any other wavelength. The two blobs might be due to an earlier AGN-related outflow, because AGNs can turn off and on as well as change direction. However, the age of a previous outflow would be much beyond the synchrotron lifetime (see above). In the case of a continuous galactic wind expanding from the disk, one would expect that the outflow of particles and magnetic field is equally strong on both sides of the spiral arm. The asymmetric distribution suggests that the outflow is not homogeneous, but emerges from individual star-forming complexes that are located not exactly in the disk plane. The non-detection of the NE counterpart on the other hand, could be caused by intrinsic depolarization due to the overlapping with the material coming from the nuclear outflow in that area.

We conclude that NGC 4388 hosts a collimated nuclear outflow and a galactic wind originating mainly from the spiral arms.

4.5. Halo pressure

The halo pressure can have several components: thermal gas pressure, magnetic pressure, cosmic ray pressure, and ram pressure from the galactic outflow. The thermal pressure of the hot gas of $P_{\text{th}} = nkT \cong (3 \pm 2) \times 10^{-12} \text{ dyn cm}^{-2}$ is estimated using a temperature of $kT = (0.5 \pm 0.3) \text{ keV}$ and a density of $n \cong (4 \pm 2) \times 10^{-3} \text{ cm}^{-3}$ from Weżgowiec et al. (2011), Table 3, interpolated between disk and tail, assuming a volume filling factor of 0.5. With an expansion velocity of $(270 \pm 70) \text{ km s}^{-1}$, the ram pressure of the galactic

wind is $P_{\text{wrip}} = 0.61 n_{\text{MH}} v^2 \cong (3 \pm 2) \times 10^{-12} \text{ dyn cm}^{-2}$. With an equipartition magnetic field strength of $B \cong (11 \pm 2) \mu\text{G}$ the magnetic pressure² is $P_B \cong B^2/(8\pi) \cong (5 \pm 2) \times 10^{-12} \text{ dyn cm}^{-2}$. Thus, there is approximate equipartition between the different pressure components (except for the cosmic ray pressure that is one third of the magnetic pressure in case of energy equipartition). If the pressure components can be simply added, the total pressure is about $1.3 \times 10^{-11} \text{ dyn cm}^{-2}$. If, however, the pressure components are not co-spatial or some of the pressure fluctuations are anticorrelated, they should not be added to a total pressure value. Hence, the pressure in the halo is in the range of $P_{\text{halo}} \cong 3\text{--}13 \times 10^{-12} \text{ dyn cm}^{-2}$.

The equipartition between the ram pressure of the outflow and the thermal pressure can be understood by the interplay between shocks and the ambient halo gas, which keeps the outflow velocity close to the sound speed of the hot halo gas.

A large-scale magnetic field may exist in the entire halo of NGC 4388 (a magnetosphere), but is observable only in regions into which a sufficiently large number of CREs is supplied from the disk by an outflow. Evidence for a large-scale regular field in the halo has to come from measurements of Faraday depth at lower frequencies with good resolution in Faraday space, i.e. a wide coverage in λ^2 space, which is not the case for the present observations centered at 6 GHz. Polarization observations in L band (centered at 1.5 GHz) are strongly affected by Faraday depolarization, hence VLA S band (centered at 3 GHz) seems more promising. A lack of Faraday rotation around 3 GHz would support the idea of stretched field loops.

4.6. ICM ram pressure

In the first part of this subsection the ICM ram pressure is estimated via the HI stripping radius, the thermal pressure of the resisting ISM and via a detailed comparison between observations and dynamical simulations. Magnetic pressure may help to resist ICM ram pressure. Its importance is investigated in the second part of this subsection. As a consistency check, the lower limit of the ICM ram pressure can be estimated via ionized high-velocity filaments that are accelerated by ram pressure. All ram pressure estimates yield values in excess of the pressure in the galactic halo. We suggest that the observed ICM clumpiness can account for this discrepancy, i.e. the galaxy is moving a portion of the clumpy ICM where the local density is several times lower than value predicted by a continuous smooth ICM distribution.

4.6.1. Ram pressure estimates

NGC 4388 is moving to the southwest. Therefore, we expect ram pressure compression in the southern part of the galactic disk. Vollmer (2009) described a scenario where the peak of ram pressure for this galaxy has already passed but in which the galaxy is still being affected in a considerable way by the ICM. The peak of the ram pressure in NGC 4388 occurred 190 ± 30 Myr ago (Pappalardo et al. 2010) having $P_{\text{max}} \approx 5 \times 10^{-11} \text{ dyn cm}^{-2}$ (Vollmer & Huchtmeier 2003). At

²The magnetic vectors in the blobs show a magnetic field which is oriented along the wind and therefore the magnetic pressure term is smaller in this direction.

this time step the absolute velocity with respect to the cluster core is estimated to be $v \approx 2000 \text{ km s}^{-1}$ and the maximum ICM density $n_{\text{ICM}} \approx 1 \times 10^{-3} \text{ cm}^{-3}$ (Vollmer & Huchtmeier 2003 erroneously gave a maximum pressure three times higher than the actual value). The model predicts that the galaxy is now affected by a ram pressure of 1/5 of the peak ram pressure occurred in the past. This means that at the present day this value would be $P \approx 1 \times 10^{-11} \text{ dyn cm}^{-2}$. Roediger et al. (2006) performed high-resolution 3D hydrodynamical simulations, using different parameters of densities and velocities, to reproduce the stripped gas as result of the interaction between a massive galaxy and the ICM. In this study, the authors were also able to reproduce outflows of about 100 kpc extension. From all the scenarios considered, they concluded that the most similar one to the case of NGC 4388 can be described by a ram pressure of a few $10^{-11} \text{ dyn cm}^{-2}$. However, improved hydrodynamical models by Roediger & Brüggen (2008) could not explain the shape of the gas tails of NGC 4388, possibly because the ICM is inhomogeneous or the outflow influences the interaction between the galaxy and the ICM. All these ram pressure estimates are based on the assumption that the spatial distribution of the ICM is continuous and smooth.

As a consistency check we apply the method of Vikhlinin et al. (2001) to calculate the ICM density. The ratio between the thermal pressure at the stagnation point P_0 and the thermal pressure of the freely streaming ICM P_{ICM} is a function of the galaxy's Mach number \mathcal{M} :

$$\frac{P_0}{P_{\text{ICM}}} = \left(\frac{\gamma + 1}{2} \right)^{(\gamma+1)/(\gamma-1)} \mathcal{M}^2 \left[\gamma - \frac{\gamma - 1}{2\mathcal{M}^2} \right]^{-1/(\gamma-1)}, \quad (3)$$

where $\gamma = 5/3$ is the adiabatic index of the monoatomic gas. With an ICM temperature of 2.2 keV (Böhringer et al. 1994) the ICM sound speed is approximately $c_{\text{ICM}} \approx 750 \text{ km s}^{-1}$. We assume a galaxy velocity within the Virgo cluster of $v_{\text{gal}} \approx 1700 \text{ km s}^{-1}$. The Mach number thus is $\mathcal{M} \approx 2.3$, leading to a pressure ratio of $P_0/P_{\text{ICM}} \approx 8$. Assuming equilibrium between the thermal pressure of the hot gas halo of the galaxy and the ICM gas at the stagnation point, we can replace P_0 by the halo pressure. With the thermal pressure of the halo P_{th} from Sect. 4.5, we obtain an ICM thermal pressure of $P_{\text{ICM}} \approx 4 \times 10^{-13} \text{ dyn cm}^2$ and an ICM density of $n_{\text{ICM}} \approx 1 \times 10^{-4} \text{ cm}^{-3}$. This agrees with the density derived from X-rays (Urban et al. 2011) and from the Sunyaev-Zel'dovich (SZ) signal measured by *Planck* (Planck Collaboration et al. 2015), while the dynamical model yields an ICM density of $n_{\text{ICM}}^{\text{model}} \approx 3 \times 10^{-4} \text{ cm}^{-3}$.

The model density thus seems to be overestimated by a factor of about 3. However, magnetic fields are not taken into account in the ICM pressure estimate of Eq. 3. Including magnetic fields will increase the estimated ICM ram pressure and thus the estimated ICM density. In Sect. 4.6.4 we show that ICM clumping might also mitigate the discrepancy between the two ICM pressure estimates.

Radio continuum observations of other Virgo galaxies affected by ram pressure like NGC 4402 or NGC 4501 also show signs of interaction with the ICM: both galaxies show a truncated gas disk (Chung et al. 2009) with

enhancements of polarization and sharp edges of the total power emission on one side of the galactic disk (Vollmer et al. 2007, 2010). Vollmer et al. (2008) estimated a ram pressure of $P \approx 8.2 \times 10^{-12} \text{ dyn cm}^{-2}$ for NGC 4501. For NGC 4402 we can estimate an upper limit of ram pressure by assuming that the western H I tail is pushed to higher galactic latitudes. According to Gunn & Gott (1972) the gravitational restoring force balances ram pressure: $P_{\text{ram}} = \Sigma v_{\text{rot}}^2 / R$. With a rotation velocity of $v_{\text{rot}} \approx 150 \text{ km s}^{-1}$, a gas surface density of $\Sigma \approx 10 M_{\odot} \text{ pc}^{-2}$, and an H I radius of $R_{\text{HI}} \approx 7.7 \text{ kpc}$ the ram pressure of NGC 4402 is $P_{\text{ram}} \approx 3.2 \times 10^{-11} \text{ dyn cm}^{-2}$. If the H I tail is ram pressure stripped gas that now falls back to the galactic disk the actual ram pressure would be a factor of few lower than our estimate.

The estimated ram pressure of NGC 4388 is somewhat smaller than that of NGC 4402 and similar to that of NGC 4501. Since these galaxies show sharp edges of the radio continuum distribution and polarized ridges on one side of the galactic disk, we would expect to see the same phenomenon in NGC 4388.

4.6.2. Magnetic pressure

In contrast to NGC 4402 or NGC 4501, the radio halo of NGC 4388 does not show a sharp southern edge. In addition, the polarized southwestern blob clearly belongs to the radio halo and thus implies that it is not compressed by ram pressure. The southern filament with a stronger magnetic field seems also unaffected by ram pressure. As observed in NGC 4569 (Chyży et al. 2006) the pressure of a galactic wind superbubble of NGC 4388 (Sect. 4.5) may resist ram pressure.

The magnetic pressure of a strong magnetic field may prevent ram pressure from removing the magnetic features seen in the halo. For that reason we estimate the magnetic field needed to balance the model ram pressure of $P_{\text{ram}} \approx 1 \times 10^{-11} \text{ dyn cm}^{-2}$. Setting this ram pressure equal to the magnetic energy density, a total magnetic field of about $16 \mu\text{G}$ is obtained. The value obtained from our observations in the southern blob is $(11 \pm 2) \mu\text{G}$ (Table 3), smaller than what is needed to balance ram pressure, so that we would not expect any extensions of the magnetic field toward the southern halo.

We also consider the possibility that energy equipartition between total cosmic rays and total magnetic fields is not valid in the halo, e.g. because the magnetic field in the expanding wind flow is highly ordered. A close coupling of the cosmic rays to the field needs scattering at field irregularities, which may be less efficient in the halo. As a result, the cosmic rays may stream with respect to the field with a velocity higher than the Alfvén speed.

A field strength resisting the ram pressure of the model by Vollmer (2009) would mean that the magnetic energy density has to be larger than the equipartition value by at least a factor of $(16 \mu\text{G}/11 \mu\text{G})^2 \approx 2$. To provide the same synchrotron intensity as in the equipartition case, the energy density of the total cosmic rays has to be lower by a factor of $2^{-(1+\alpha)} \approx 0.25$ (for a synchrotron spectral index $\alpha \approx 1$). The corresponding ratio between the magnetic and cosmic-ray energy densities is $\gtrsim 2^{(2+\alpha)} \approx 8$, which is an extreme deviation from equipartition, causing dynamical effects that lead to recovery of equilibrium.

Another argument against a super-equipartition field of $16 \mu\text{G}$ field in the halo comes from the synchrotron lifetime of CREs that would decrease to about 7 Myr. An unrealistically high average outflow speed of 500 km s^{-1} would be needed to reach the height of the blobs above the disk plane.

We conclude that the estimates of the field strengths in Table 3 are realistic. Either the ram pressure cannot be balanced by the magnetic pressure alone or the modeled ram pressure is overestimated.

4.6.3. Ionized high velocity filaments

In the following, we will estimate a lower limit for the ram pressure needed to accelerate clumps of ionized gas observed by Yoshida et al. (2004). The “West High Velocity Filaments” contain several subclumps which are located east of the galactic disk outside the faint $\text{H}\alpha$ halo. The radial velocities of the clumps in the filaments are between -250 and -360 km s^{-1} with respect to the systemic velocity of NGC 4388. The radial components of the rotation velocity in these regions have positive values. Since the galaxy is leaving the cluster, the ionized clumps are decelerated by ram pressure of the ICM to negative velocities. The acceleration of a gas clump is given by $a = P_{\text{ram}}/\Sigma$, where Σ is the column density of the clump. The acceleration is approximately $a = \Delta v/\Delta t = (\Delta v)^2/L$, where L is the distance over which the clump is accelerated. We assume $\Delta v \geq 350 \text{ km s}^{-1}$ and $L \cong 5 \text{ kpc}$. For the column density we take the mean gas density³ of $n_{\text{clump}} \cong 0.04 \text{ cm}^{-3}$ and a size of $s = 100 \text{ pc}$ given by Yoshida et al. (2002). In this way we estimate the minimum ram pressure to accelerate the ionized clouds to the observed velocities to be $P_{\text{low}} \geq \rho s(\Delta v)^2/L \cong 1.6 \times 10^{-12} \text{ dyn cm}^{-2}$, a factor of 2 lower than the individual halo pressure terms estimated in Sect. 4.5. This lower limit is consistent with ram pressure being equal or somewhat lower to the halo pressure due to the galactic wind.

4.6.4. ICM clumpiness

From the previous sections, there are indications that the ICM ram pressure from the numerical models (Vollmer 2009, Roediger et al. 2006) may be overestimated by a factor of several at this cluster radius.

X-ray spectroscopy of the Virgo cluster (Urban et al. 2011) indicates a drastic drop of temperature and metallicity beyond a radius of $r \cong 450 \text{ kpc}$ from the cluster center. A natural explanation for this decrease is clumping of the ICM that sets in at that radius. Based on the detailed comparison between observations and dynamical models Vollmer (2009) determined the 3D distance of the Virgo spiral galaxies. With respect to the cluster center, the 3D distance of NGC 4388 is estimated to be 420 kpc. This distance compares well with the distance where the ICM becomes clumpy. We note that due to clumpiness the actual ICM ram pressure acting on NGC 4388 might be up to a factor of two lower than what is expected from a model including a smooth continuous ICM.

The *Planck* measurements of the Virgo cluster SZ effect (Planck Collaboration et al. 2015) show that radially averaged ICM clumping cannot be strong at the

cluster distance of 420 kpc. Based on numerical simulations, typical radially averaged clumping factors $C = \langle n_e^2 \rangle / \langle n_e \rangle^2$ of unrelaxed clusters are $C = 1.5 - 2$ (Zhuravleva et al. 2013). Locally, the density can be enhanced by a factor of 3 – 10. However, locations with densities exceeding three times the mean density are extremely rare (see Fig. 3 of Zhuravleva et al. 2013).

With a galaxy velocity of 1700 km s^{-1} and an ICM density of $n_{\text{ICM}} \cong 1 \times 10^{-4} \text{ cm}^{-3}$ (Urban et al. 2011), the ICM ram pressure is $P_{\text{ram}} \cong 3 \times 10^{-12} \text{ dyn cm}^{-2}$ which is consistent with the thermal halo pressure (Sect. 4.5). If the magnetic and CR pressures are co-spatial with the thermal halo pressure, the actual ICM ram pressure can exceed $3 \times 10^{-12} \text{ dyn cm}^{-2}$. On the other hand, the dynamical model predicts an ICM ram pressure of $1 \times 10^{-11} \text{ dyn cm}^{-2}$. Thus, ICM clumping cannot be excluded and the actual ICM ram pressure acting on NGC 4388 might well be a few times higher than the radially averaged ICM density estimated from X-ray and SZ observations.

Current dynamical simulations of ram pressure stripping events assume a continuous ICM distribution (Vollmer et al. 2001, Roediger et al. 2006, Tonnesen & Bryan 2009). The influence of a clumpy ICM on these simulation depends on the stage of the interaction: a clumpy ICM distribution significantly affects only the beginning and the end of the simulations when the distance to the Virgo cluster center of the galaxy exceeds $\approx 500 \text{ kpc}$. If the galaxy is observed close to or after peak ram pressure the changes of the simulation results with respect to a continuous ICM distribution are expected to be minor. However, if the galaxy is observed at the beginning of the ram pressure stripping event or more than 200 Myr after peak ram pressure, the clumpy ICM distribution will have a significant influence on gas distribution and velocity.

5. SUMMARY

Our new VLA 6 GHz broad-band observations of the edge-on Virgo cluster galaxy NGC 4388 allowed us to reach unprecedented low noise levels, revealing striking new details of this object. The polarized emission obtained for the first time for this galaxy with RM synthesis, show extensions of the magnetic field toward the outskirts of the galaxy, indicating a connection between disk and halo. Two polarized filamentary structures appear at the end of both northern and southern nuclear outflows which correlate with $\text{H}\alpha$ and X-ray observations. The change in orientation of the magnetic vectors in the southern spiral arm reveals for the first time the southern nuclear outflow. Furthermore, two horizontally extended blobs of polarized emission are observed in the halo, about 2 kpc above and below the northeastern and southwestern spiral arms, respectively. Within these blobs, the ordered magnetic field is oriented perpendicular to the galactic disk.

The comparison between multi-wavelength observations of prototype galactic winds shows that NGC 4388 does not host a symmetric central galactic wind. However, we suggest that, together with $\text{H}\alpha$, X-ray, and total power emission being located closer to the spiral arms within the halo, the blobs of polarized emission trace a galactic wind, which most likely originate from separate sources in the spiral arms. In such a scenario the CREs

³This implies a volume filling factor of 10^{-3}

travel from the spiral arms into the halo, reaching distances of up to $\cong 3.3$ kpc in the plane of the sky. Assuming equipartition between CR particles and the magnetic field we estimate a total magnetic field strength for the different parts of the galaxy taking into account individual spectral indices and pathlengths. In particular, our estimate of the total magnetic field strength for the polarization blobs is $(11 \pm 2) \mu\text{G}$. With this magnetic field strength, the synchrotron lifetime of electrons in the polarized blob is $\cong (12 \pm 3) \text{ Myr}$. For traveling a distance of $\cong 3.3$ kpc, the average outflow velocity of those particles is $(270 \pm 70) \text{ km s}^{-1}$, which agrees with the typical speed of a galactic wind expanding from the spiral arms into the halo.

Another edge-on Virgo galaxy, NGC 4402, shows a sharp edge in the radio continuum emission which is interpreted as a compressed galactic halo. The observed symmetry of the polarized halo features in NGC 4388 excludes a compression of the halo gas by ICM ram pressure. We estimate the halo magnetic pressure and the ram pressure of the galactic wind to be $P_{\text{halo}} \approx 3 \times 10^{-12} \text{ dyn cm}^{-2}$. This pressure is comparable to the thermal pressure derived from X-ray observations.

The estimate of the ICM ram pressure based on the galaxy velocity from dynamical models and a radially averaged ICM density profile from X-ray observations yields $P_{\text{ICM}} \cong 3 \times 10^{-12} \text{ dyn cm}^{-2}$, in agreement with our estimate of the thermal halo pressure. If magnetic fields are ubiquitous in the halo, the halo pressure estimate increases.

Allowing for ICM clumping, the actual ram pressure acting on NGC 4388 might be up to few times higher than

what is expected based on a given galaxy velocity and an ICM density determined from X-ray and SZ observations.

NGC 4388 besides NGC 4569 (Chyży et al. 2006) is the second galaxy in the Virgo cluster which shows a galactic outflow resisting ICM ram pressure. The detection of a radio halo around other cluster spiral galaxies could be used for an estimate of ICM density and ram pressure within a factor of a few.

Further observations at lower frequencies (GMRT, LO-FAR, SKA) will reveal stronger total intensity emission from the halo of this galaxy allowing us to do a spectral index analysis and therefore better constrain the aging of the CREs. Measurements of the large-scale structure of the halo magnetic field in NGC 4388 with help of polarization data are needed, e.g. with the VLA S band where good resolution in Faraday space can be reached. $\text{H}\alpha$ observations are also crucial to constrain the velocities within the polarized blobs. We expect to see blue-shifted emission in the wind of the southern part and red-shifted in the northern part due to the inclination of the galaxy towards the observer.

This work has used the Karl G. Jansky Very Large Array operated by The National Radio Astronomy Observatory (NRAO). The NRAO is a facility of the National Science Foundation operated under cooperative agreement by Associated Universities, Inc.

We thank the anonymous referee for useful comments. We also thank Aritra Basu, Marcus Brüggen, Klaus Dolag, Christian Fendt, Stefanie Komossa, and Robert Laing for useful discussions.

We acknowledge support by project DFG RU1254.

REFERENCES

- Adebahr, B., Krause, M., Klein, U., et al. 2013, *A&A*, 555, A23
 Arribas, S., Colina, L., Bellocchi, E., Maiolino, R., & Villar-Martín, M. 2014, *A&A*, 568, A14
 Arshakian, T. G., & Beck, R. 2011, *MNRAS*, 418, 2336
 Beck, R. 2001, *Space Sci. Rev.*, 99, 243
 —. 2007, *A&A*, 470, 539
 Beck, R., & Krause, M. 2005, *Astronomische Nachrichten*, 326, 414
 Beck, R., & Wielebinski, R. 2013, in *Planets, Stars and Stellar Systems. Volume 5: Galactic Structure and Stellar Populations*, ed. T. D. Oswalt & G. Gilmore, 641
 Böhringer, H., Briel, U. G., Schwarz, R. A., et al. 1994, *Nature*, 368, 828
 Brentjens, M. A., & de Bruyn, A. G. 2005, *A&A*, 441, 1217
 Cayatte, V., van Gorkom, J. H., Balkowski, C., & Kotanyi, C. 1990, *AJ*, 100, 604
 Chung, A., van Gorkom, J. H., Kenney, J. D. P., Crawl, H., & Vollmer, B. 2009, *AJ*, 138, 1741
 Chyży, K. T., Soida, M., Bomans, D. J., et al. 2006, *A&A*, 447, 465
 Dahlem, M. 1997, *PASP*, 109, 1298
 Falcke, H., Wilson, A. S., & Simpson, C. 1998, *ApJ*, 502, 199
 Giroletti, M., & Panessa, F. 2009, *ApJ*, 706, L260
 Gunn, J. E., & Gott, I. J. R. 1972, *ApJ*, 176, 1
 Heald, G. 2009, in *IAU Symposium, Vol. 259, IAU Symposium*, ed. K. G. Strassmeier, A. G. Kosovichev, & J. E. Beckman, 591–602
 Heald, G. 2015, in *Astrophysics and Space Science Library, Vol. 407, Magnetic Fields in Diffuse Media*, ed. A. Lazarian, E. M. de Gouveia Dal Pino, & C. Melioli, 41
 Heesen, V., Beck, R., Krause, M., & Dettmar, R.-J. 2009, *A&A*, 494, 563
 Hummel, E., & Saikia, D. J. 1991, *A&A*, 249, 43
 Hummel, E., van Gorkom, J. H., & Kotanyi, C. G. 1983, *ApJ*, 267, L5
 Irwin, J., Beck, R., Benjamin, R. A., et al. 2012, *AJ*, 144, 43
 Iwasawa, K., Wilson, A. S., Fabian, A. C., & Young, A. J. 2003, *MNRAS*, 345, 369
 Kellermann, K. I., Kovalev, Y. Y., Lister, M. L., et al. 2007, *Ap&SS*, 311, 231
 Krause, M. 2011, *ArXiv e-prints*, arXiv:1111.7081
 Kukulka, M. J., Pedlar, A., Baum, S. A., & O’Dea, C. P. 1995, *MNRAS*, 276, 1262
 Kuo, C. Y., Braatz, J. A., Condon, J. J., et al. 2011, *ApJ*, 727, 20
 Li, J.-T., Li, Z., Wang, Q. D., Irwin, J. A., & Rossa, J. 2008, *MNRAS*, 390, 59
 Oosterloo, T., & van Gorkom, J. 2005, *A&A*, 437, L19
 Pappalardo, C., Lançon, A., Vollmer, B., et al. 2010, *A&A*, 514, A33
 Pearson, T. J., & Zensus, J. A. 1987, in *Superluminal Radio Sources*, ed. J. A. Zensus & T. J. Pearson, 1–11
 Planck Collaboration, Ade, P. A. R., Aghanim, N., et al. 2015, *ArXiv e-prints*, arXiv:1511.05156
 Ranalli, P., Comastri, A., Origlia, L., & Maiolino, R. 2008, *MNRAS*, 386, 1464
 Roediger, E., & Brüggen, M. 2008, *MNRAS*, 388, 465
 Roediger, E., Brüggen, M., & Hoeft, M. 2006, *MNRAS*, 371, 609
 Soida, M., Krause, M., Dettmar, R.-J., & Urbanik, M. 2011, *A&A*, 531, A127
 Sokoloff, D. D., Bykov, A. A., Shukurov, A., et al. 1998, *MNRAS*, 299, 189
 Strickland, D. K., Heckman, T. M., Weaver, K. A., Hoopes, C. G., & Dahlem, M. 2002, *ApJ*, 568, 689
 Strickland, D. K., Ponman, T. J., & Stevens, I. R. 1997, *A&A*, 320, 378
 Tonnesen, S., & Bryan, G. L. 2009, *ApJ*, 694, 789
 Urban, O., Werner, N., Simionescu, A., Allen, S. W., & Böhringer, H. 2011, *MNRAS*, 414, 2101
 Velleux, S., Bland-Hawthorn, J., Cecil, G., Tully, R. B., & Miller, S. T. 1999, *ApJ*, 520, 111

- Vikhlinin, A., Markevitch, M., & Murray, S. S. 2001, *ApJ*, 551, 160
- Vollmer, B. 2009, *A&A*, 502, 427
- Vollmer, B., Cayatte, V., Balkowski, C., & Duschl, W. J. 2001, *ApJ*, 561, 708
- Vollmer, B., & Huchtmeier, W. 2003, *A&A*, 406, 427
- Vollmer, B., Soida, M., Beck, R., et al. 2013, *A&A*, 553, A116
- . 2007, *A&A*, 464, L37
- Vollmer, B., Soida, M., Chung, A., et al. 2010, *A&A*, 512, A36
- . 2008, *A&A*, 483, 89
- Weżgowiec, M., Urbanik, M., Beck, R., Chyży, K. T., & Soida, M. 2012, *A&A*, 545, A69
- Weżgowiec, M., Vollmer, B., Ehle, M., et al. 2011, *A&A*, 531, A44
- Wiegert, T., Irwin, J., Miskolczi, A., et al. 2015, *AJ*, 150, 81
- Yoshida, M., Yagi, M., Okamura, S., et al. 2002, *ApJ*, 567, 118
- Yoshida, M., Ohshima, Y., Iye, M., et al. 2004, *AJ*, 127, 90
- Zhuravleva, I., Churazov, E., Kravtsov, A., et al. 2013, *MNRAS*, 428, 3274